Variation Evaluation of Path Characteristic and Site Amplification Factor of Earthquake Ground Motion at Four Sites in Central Japan

Takashi Nagao
Research Center for Urban Safety and Security
Kobe University
Kobe City, Japan
nagao@people.kobe-u.ac.jp

Abstract-The considered parameters in seismic design vary, with the Earthquake Ground Motion (EGM) having the largest variation. Since source characteristic, path characteristic, and Site Amplification Factor (SAF) influence the EGM, it is crucial to appropriately consider their variations. Source characteristic variations are mainly considered in a seismic hazard analysis, which is commonly used to evaluate variations in EGM. However, it is also important to evaluate variations in path characteristic and SAF with only a few studies having individually and quantitatively examined the variations of these two characteristics. In this study, based on strong-motion observation records obtained from four sites in central Japan, the three characteristics were extracted from seismograms using the concept of spectral inversion. After removing the source characteristic, the path characteristic and SAF were separated, and the variations in these two characteristics were quantified. To separate and obtain each characteristic from the observed record, one constraint condition must be imposed, whereas the variations in the constraint condition must be ignored. In that case, the variations in the constraint condition are included in the variations of the separated characteristics. In this study, this problem was solved by evaluating the variation in the constraint condition, which is the SAF at a hard rock site, by the use of the vertical array observation record at the site.

Keywords-earthquake ground motion; path characteristic; site amplification factor; variation

I. INTRODUCTION

In seismic design, the cross-section of a structure is determined in such a way that the cross-sectional resistance exceeds the section force caused by an earthquake. Since the parameters to be considered in seismic design vary, the cross-section of a structure should be set considering the possibility that the seismic load acting on the structure exceeds the design value. The Earthquake Ground Motion (EGM) has the largest variation among the considered parameters in seismic design. Therefore, it is critical to accurately evaluate the variation in EGM. Seismic hazard analysis [1] is a method for considering variations in EGM. In seismic hazard analysis, probabilistic EGM is evaluated by considering variations in parameters such as seismic magnitude and hypocenter location.

EGM is determined by three characteristics: source characteristic, path characteristic, and Site Amplification Factor (SAF). These three characteristics must be considered carefully because the EGM varies significantly depending on the evaluation method of these characteristics [2]. In seismic hazard analysis, source characteristic is the major variation evaluation object, and path characteristic and SAF are treated deterministically. However, since these two characteristics vary in reality, it is necessary to evaluate the variations in path characteristic and SAF separately in order to conduct rational seismic design. Although there are many research cases on the variation in amplification characteristics, the definitions of amplification characteristics vary, such as the ratio of spectral acceleration to the predicted value by ground motion prediction equations [3], the amplification at the object location with respect to the reference location [4], the ratio of the vertical array strong-motion observation record on the ground surface to the borehole [5, 6], and the residual of the observed EGM to the probabilistically evaluated EGM [7]. The SAF to be considered when the EGM is separated into the three characteristics must include not only the amplification by the shallow subsurface but also that by the deep subsurface, because the amplification factor by a shallow subsurface is significantly smaller than the actual SAF [8, 9]. Therefore, the variation in SAF for each frequency, including the effect of deep subsurface must be evaluated.

There are cases in which the variations of SAF, including the effect of deep subsurface, were studied using the spectral ratio of seismograms observed at two sites [10, 11]. However, these studies did not separate path characteristic and SAF, and because path characteristic was treated deterministically, their results included variations of path characteristic and SAF. There are no case studies in which the variations in path characteristics and SAF were quantified after separation. Spectral inversion [12, 13] is a technique for separating each characteristic from the observed records. The current study separates path characteristic and SAF based on the concept of spectral inversion and conducts quantitative evaluation of each variation.

Corresponding author: Takashi Nagao

II. METHOD

A. Target Sites and Target Earthquakes

This study focuses on four sites (GIFH20, GIFH24, GIFH28, and NGNH20) in central Japan that are part of the KiK-net [14] strong-motion seismograph network as shown in Figure 1. KiK-net provides EGMs recorded at the ground surface and in the borehole simultaneously, and P-S logging reveals the S-wave velocity profile leading to the seismograph installation position in the borehole. Strong-motion records and ground data were made available to the public by [15]. However, seismographs in boreholes are rarely installed at seismic bedrock in which S-wave velocity exceeds 3km/s. Therefore, the S-wave velocity profile from the ground surface to the seismic bedrock was obtained by combining the information from KiK-net and J-SHIS [16] as described in [8]. The obtained S-wave velocity profiles are shown in Figure 2. Among the sites, GIFH28 has the thickest and NGNH20 the thinnest sediment site. In GIFH24, the depth at which the S-wave velocity exceeds 1500m/s is shallower than that in NGNH20. The multiple reflection theory calculates transfer functions assuming horizontally stratified ground conditions (Figure 3). In the frequency range of 0.1–10Hz, which is important in seismic engineering, the amplification factor of GIFH24 is the smallest with values less than 2 in the frequency range lower than 7Hz. Because the soil layer thickness with an S-wave velocity of 720m/s is relatively thick (= 25m), the amplification factor is as high as 5 at 6Hz in NGNH20. First-order peaks occur at 2Hz in GIFH20 and 0.6Hz in GIFH28, in which the sedimentary layer is the thickest.

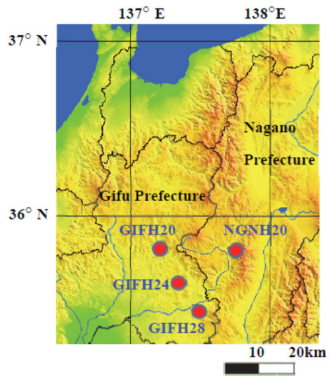

Fig. 1. Target sites.

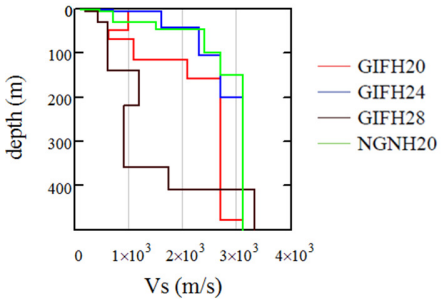

Fig. 2. S-Wave velocity profiles.

Table I shows the list of the considered events. The epicenters of the target events, as well as the locations of the observation sites, are shown in Figure 4. The red circles indicate seismograph installation sites, and the blue cross marks indicate the epicenters. The epicenters do not exist on the west side of the observation sites, but they are distributed evenly in the other directions.

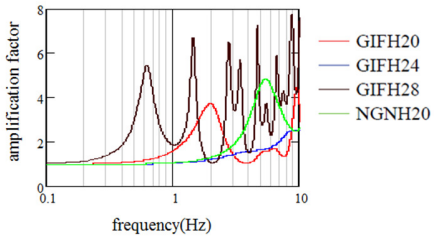

Fig. 3. Transfer functions.

TABLE I. TARGET EARTHQUAKES

No	Date	Time	Lon (deg)	Lat (deg)	Depth (km)	*M*	Site*
1	Sep/27/2020	13:13	137.80	35.10	45	5.3	b, c, d
2	Apr/23/2020	13:44	137.32	35.64	3	5.5	b, d
3	Feb/13/2018	14:39	137.59	35.87	3	4.1	b, c, d
4	Dec/6/2017	00:13	137.97	36.38	10	5.3	b, d
5	Jun/25/2017	07:02	137.59	35.87	7	5.6	b, c, d
6	Dec/6/2016	09:05	137.34	36.01	5	4.5	b, c, d
7	May/25/2015	14:28	139.64	36.05	56	5.5	a, b, d
8	Mar/4/2015	00:04	136.80	35.34	40	4.6	a, b, c
9	Dec/3/2014	23:19	137.12	35.29	45	4.2	a, b, c, d
10	Sep/16/2014	12:28	139.86	36.09	47	5.6	a, b, d
11	Jun/1/2012	17:48	139.88	36.03	44	5.1	a, b, c, d
12	Apr/25/2012	05:22	140.68	35.72	43	5.5	a, b, d
13	Jan/28/2012	07:43	138.98	35.49	18	5.4	a, b, c, d
14	Jun/30/2011	08:21	137.95	36.19	4	5.1	a, b, d
15	Apr/16/2011	11:19	139.94	36.34	79	5.9	a, b, c, d
16	Mar/16/2011	03:33	137.30	36.00	0	4.0	a, b, c, d

* a: GIFH20, b: GIFH24, c: GIFH28, d: NGNH20

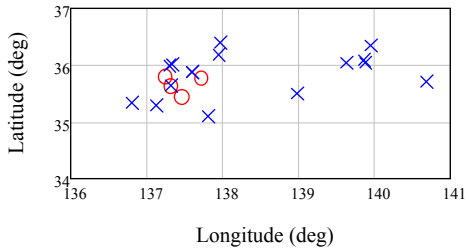

Fig. 4. Target Sites and epicenters.

Because EGM records of small seismic magnitude (*M*) have a low signal-to-noise (S/N) ratio, events of seismic magnitude M = 4.0 or larger are considered. Additionally, EGM records of M = 6.0 or larger are excluded to avoid the effect of the rapture process at the fault plane. With the ω^{-2} model [17], only EGM records with good S/N ratios in the range of 0.3Hz or higher were used. To discuss the amplification characteristics of S-waves, 10.24s records were extracted for the S-wave arrival. Before calculating the Fourier spectra, baseline correction was conducted, and the extracted

records were tapered. Based on the root mean square of the Fourier spectra of seismograms recorded horizontally in two directions, a Parzen window with a bandwidth of 0.3Hz was used to smooth the spectra.

B. Separation Method of the Three Characteristics

The three characteristics are separated from the observed records according to the concept of spectral inversion. This study focuses on seismograms of the same event recorded at multiple stations. The Fourier spectra of the observed records can be expressed as the product of the source characteristic, path characteristic, and SAF as shown in (1):

$$O_{ij}(f) = S_i(f)P_{ij}(f)G_j(f) \quad (1)$$

where O is the observed EGM, S is the source characteristic, P is the path characteristic, G is the SAF, i is the event number, j is the station number, and f is the frequency. The values of each characteristic for each frequency can be obtained by solving the equations simultaneously using (2) in which the equation is expressed as a common logarithm.

$$\log O_{ij} = \log S_i + \log P_{ij} + \log G_j \quad (2)$$

The path characteristic can be expressed by (3):

$$P_{ij}(f) = \frac{1}{r_{ij}^{\,n}} exp\left(-\pi f r_{ij} / QVs\right) \quad (3)$$

where r is the hypocentral distance and n is a value representing the geometric attenuation of the body wave, with its typical value being 1.0, but it is pointed out that $n = 2$ when the hypocentral distance is significantly long [18]. In this study, $n = 2$ was assumed for a dataset with hypocentral distances of 120km or more. Vs is the average S-wave velocity along the propagation path, and $Vs = 3.8$km/s in the target area. Q is the Q-value, which represents the inelastic attenuation of EGM.

There is a trade-off relationship among the characteristics: for example, a product of large path characteristics and small SAF can result in the same value as a product of small path characteristics and large SAF. Therefore, one constraint condition must be imposed to solve the equations simultaneously. The constraint condition is set as the SAF at one station and calculated as a theoretical SAF assuming one-dimensional (1D) ground structure [19]. The SAF of a significantly small rock site is chosen for the constraint condition. However, even at rock sites, EGM is amplified in many cases because of weathering [20]. Furthermore, because of the heterogeneity of a three-dimensional (3D) ground structure, the SAF assuming 1D ground structures often underestimates the actual SAF [2, 21]. Therefore, it is desirable that the SAF used as a constraint condition to be as small as possible and the S-wave velocity profile down to seismic bedrock is disclosed. As shown in Figure 3, the amplification factor at GIFH24 is significantly small in the frequency band below 10Hz, and we can assume that the difference in SAF between the actual and the one calculated by assuming a 1D structure is negligible. As a constraint condition, this study uses the 1D amplification factor (1DA) at GIFH24.

III. RESULTS AND DISCUSSION

A. SAF Variation in Low-Frequency Bands at Hard Rock Sites

Path characteristic and SAF can be separated in the spectral inversion and variations of the two characteristics can be discussed. However, the variation cannot be evaluated for the constraint condition. The constraint condition, which is the SAF at the reference hard rock site, also varies. Therefore, variations in the obtained characteristics include variations in the constraint conditions. Because seismographs are installed at the ground surface (S) and in boreholes (B) at KiK-net sites, the variation can be evaluated using the spectral ratio (S/B). However, even if the seismograph in the borehole is installed on the seismic bedrock, S/B cannot be considered as the SAF because borehole records include the upward EGM (E) and downward EGM (F), which are reflected at the layer boundary ($E + F$). Because E and F are identical on the ground surface, EGM is $2E$, and the S/B becomes $2E/(E + F)$. However, the SAF is defined as the spectral ratio of the EGM at the ground surface to that obtained by doubling the incident EGM (E) at the bedrock ($2E/2E$). Figure 5 compares the S/B ($= 2E/(E + F)$) with the SAF ($= 2E/2E$) under horizontally stratified ground conditions, using GIFH24 and NGNH20 as examples. The red line represents the SAF, and the blue line represents the S/B. Although the difference between the two is large in the frequency band higher than 1Hz, it is tiny in the frequency band lower than 1Hz. Therefore, the variation in S/B in the frequency band lower than 1Hz of these two sites is the variation in the SAF. Figure 6 shows the variation in S/B calculated with the observation record. The gray line represents the individual S/B and the red line represents the average value. Each characteristic is separated on a logarithmic scale in the spectral inversion, as shown in (2). Therefore, unless otherwise specified, these results are on a logarithmic scale hereafter. The value of S/B agrees with the theoretical value on average in the frequency band of 1Hz or lower, although there is some dispersion.

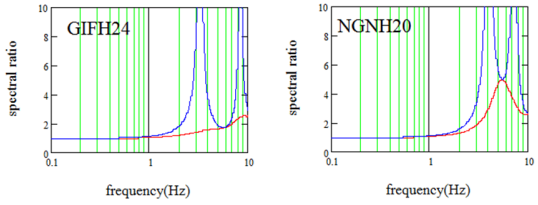

Fig. 5. Comparison of $2E/(E + F)$ and $(2E/2E)$.

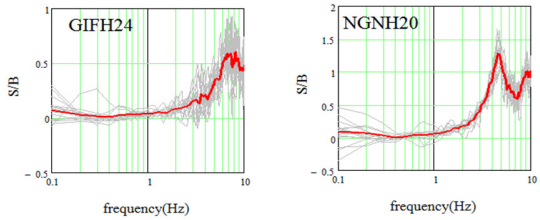

Fig. 6. Variation in S/B.

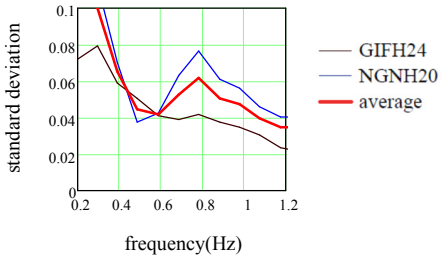

Fig. 7. SD of S/B.

Figure 7 shows the standard deviation (SD) of *S*/*B* in the frequency band lower than 1Hz. The SD is large in frequencies lower than 0.4Hz because of the poor S/N ratio in the seismograms of small amplitude. The SD of the SAF of hard rock sites in the frequency band lower than 1Hz was determined to be 0.048 using the average SD in the range of 0.488 to 1.074Hz. Figure 8 shows the histogram of the *S*/*B*, referring to the results at frequencies 0.586 and 0.781Hz. The probability distribution can be considered normal.

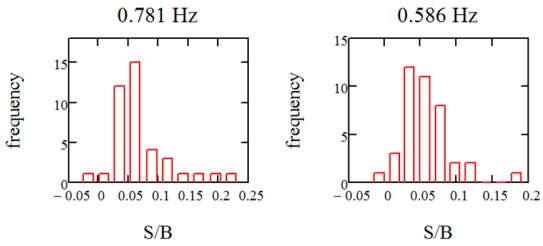

Fig. 8. Histogram of *S*/*B*.

B. Evaluation of Q-Value and Path Characteristic Variation

Because the variation in the SAF at hard rock sites was obtained when considering the frequency band of 1Hz or lower, the variation in the path characteristics can be evaluated based on the results. The *Q*-value used to evaluate path characteristics varies by region, and its frequency dependence has been mentioned. There have been no previous studies on the *Q*-value for the regions covered in this study, but the *Q*-values for other Japanese regions are $Q = 83 f^{0.73}$ [22] and $Q = 33 f^{1.0}$ [23]. In this study, we first evaluate the *Q*-value for the target area. Based on the simultaneous records from two locations (i.e. GIFH24 and NGNH20), we can evaluate the *Q*-value using (4) and combining (2) and (3).

$$Q = \frac{\pi f \left(r_j - r_k\right) log_{10} e \Big/ Vs}{log O_k - log O_j - log G_k + log G_j - n log r_j + n log r_k} \quad (4)$$

where *j* and *k* are the observation stations.

SAF in the frequency band higher than 1Hz cannot be determined at this point, but for frequencies lower than 1Hz the SAF of the two stations can be considered as 1.0. Therefore, the *Q*-value can be determined by (4). The *Q*-value was obtained as in (5) regarding the average *Q*-value for each frequency, and the minimum spectral residual, which is to be described later.

$$Q = 70 f^{0.90} \quad (5)$$

Figure 9 compares the average *Q*-value with the value obtained by (5). The blue line represents the average *Q*-value, and the red line represents the value according to (5).

The variation in path characteristic is evaluated based on the obtained *Q*-value. By applying (2) to the records of two sites *j* and *k* (i.e. GIFH24 and NGNH20), the spectral residual (*SR*) is obtained as follows:

$$SR = log O_j - log O_k - log P_j + log P_k - log G_j + log G_k \quad (6)$$

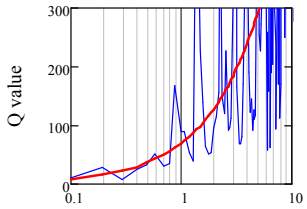

Fig. 9. *Q*-value.

The *SR* distribution is displayed in the left panel of Figure 10. The gray lines represent individual results, and the red line represents the average value. If path characteristic and SAF do not vary, *SR* becomes zero. Although the average *SR* is generally zero for frequencies lower than 1Hz, the variation in *SR* is large. The SD of *SR* is shown in the right panel of Figure 10. The average value of SD in the frequency band 0.293-1.074Hz was determined to be 0.184. The histograms of *SR* at frequencies 0.586 and 0.781Hz are shown in Figure 11. Although the result at 0.586Hz deviates from the normal distribution, the frequency distribution at 0.781Hz can be considered normal.

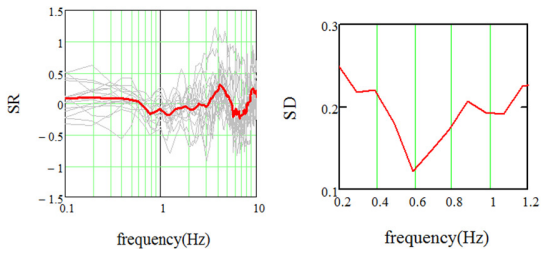

Fig. 10. Distribution and SD of *SR*.

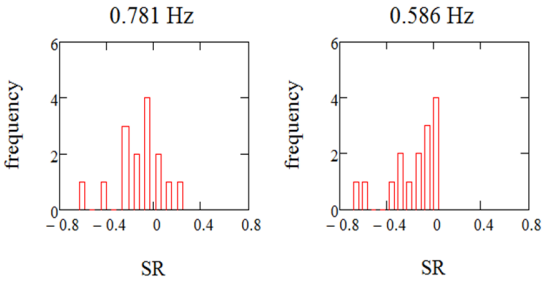

Fig. 11. Histogram of *SR*.

This *SR* variation includes the variations in path characteristics and SAFs of the two sites. Assuming that the path characteristic and SAF at each site follow independent normal distributions, the following equation holds:

$$\sigma_{SR}^{\ 2} = 2\left(\sigma_P^{\ 2} + \sigma_G^{\ 2}\right) \quad (7)$$

where σ is the SD.

By using the SD of SAF obtained in the previous section, the SD of the path characteristic was determined to be 0.121.

C. SAF and its Variation

Based on the above results, the variation in SAF at the site where the effect of the sedimentary layer cannot be ignored is evaluated. Because the path characteristics vary slightly with frequency, the SD obtained in the previous section is assumed to be applicable at all frequencies. Furthermore, because GIFH24 is a site with a significantly small amplification factor in the frequency band lower than 10Hz, it is assumed that the average value of SAF at GIFH24 agrees with the amplification factor assuming 1D ground structure (1DA) considering ground structure leading to the seismic bedrock. Regarding the variation in SAF at GIFH24, it is assumed that the SD value obtained in the previous section for the low-frequency band can be applied to all frequencies. Based on the simultaneous records at GIFH24 and NGNH20, SAF and its variations of NGNH20 are evaluated by solving (6) for SAF at NGNH20 as shown in the left panel of Figure 12. The gray lines represent the individual results, and the red line represents the average value. The right panel of Figure 12 shows the average value and the SD of SAF. The red line represents the average value and the blue line represents the SD. The SD is less dependent on the frequency. The SD has an average value of 0.323 in the 0.195–10Hz frequency band. Because the SD here includes variation in path characteristics at two sites and variation in SAF at GIFH24, these variations are removed using the same approach as in (7). The average values of the SD of SAF at NGNH20 in the frequency bands of 1–10Hz and 0.195–10Hz were determined to be 0.282 and 0.270 respectively. Furthermore, the SAF at GIFH28 is discussed. The procedures are the same as in NGNH20. The left panel of Figure 13 shows the SAF, with the gray lines representing the individual results and the red line representing the average value.

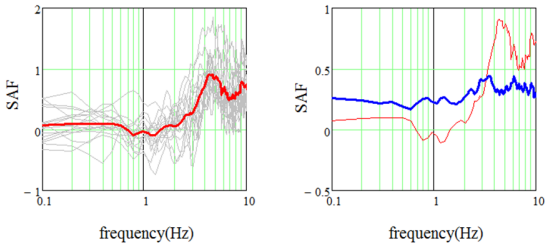

Fig. 12. Average and SD of SAF (NGNH20).

The right panel of Figure 13 shows the average SAF (red) and the SD (blue) lines. The SD in the frequency band higher than 2Hz is slightly larger than that in the lower-frequency band. The average value of SD in the frequency band of 0.195–10Hz is 0.316. When the variation in the SAF of GIFH24 and path characteristics of the two sites were removed from the SD, the average value of SD of SAF at GIFH28 was 0.061 in the 0.195–1.1Hz frequency band, 0.277 in the 1–10Hz frequency band, and 0.262 in the 0.195–10Hz frequency band.

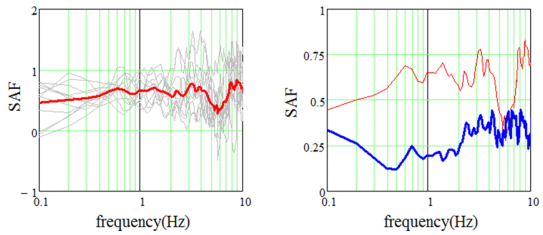

Fig. 13. Average and SD of SAF (GIFH28).

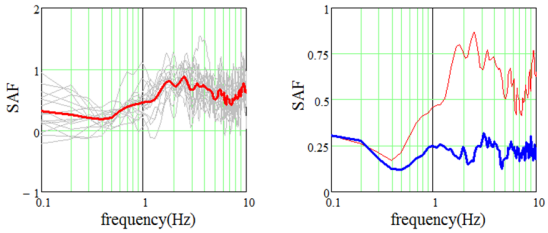

Fig. 14. Average and SD of SAF (GIFH20).

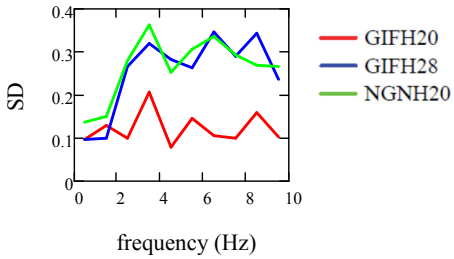

Fig. 15. Average SD of SAF.

The left panel of Figure 14 shows the SAF for GIFH20, with gray lines representing the individual results and the red line representing the average value. The right panel of Figure 14 shows the average value and SD of SAF, with the red line representing the average value and the blue line the SD. The average SD in the frequency band from 0.195 to 10Hz is 0.217. When the variation of the SAF of GIFH24 and the path characteristics of the two sites were removed from this SD, the average value of the SD of SAF at GIFH20 was 0.080 in the 0.195–1.1Hz frequency band, 0.130 in 1–10Hz, and 0.125 in 0.195–10Hz.

Because the SD at each site varies with frequency, Figure 15 shows the average SD in case of SAF with frequency. The SD is small for frequencies lower than 2Hz, in the range of 0.10 - 0.15, but a large value of approximately 0.30 can be obtained in the case of GIFH28 and NGNH20 when considering frequencies higher than 3Hz. However, at GIFH20, the SD is almost constant in all frequency bands and is smaller than those at the other two sites. The average value of SAF varies significantly with frequency at the three sites, but the SD

does not vary significantly with frequency and is not dependent on the average value of SAF. Because the SAF in the low-frequency band is mainly determined by the deep subsurface structure, a low SD of the SAF in the low-frequency band indicates a minor local change in the deep subsurface structure near the observation sites. However, the SAF in the high-frequency band mainly depends on the shallow subsurface structure, implying that the shallow subsurface structure is changing in a complex manner around the site where the SD of the SAF is large in the high-frequency band. However, the sites where the SDs of SAFs do not increase even in the case of high-frequency bands, such as in GIFH20, are considered to be sites at which the surrounding shallow subsurface structure does not change significantly.

D. Comparison of 1DA and SAF

Figure 16 compares the SAF in this study to 1DA used in design practice. The red line represents the average SAF, the blue line represents the 1DA considering shallow and deep subsurface, and the black line represents the 1DA considering shallow subsurface only. Note that those values are expressed on an arithmetic scale. Compared to the 1DA considering deep subsurface, the shallow subsurface 1DA significantly underestimates the amplification factors. This result is in accordance with the findings in [8]. Except for the second-order peak at 1.5Hz of GIFH28, the 1DA considering deep subsurface underestimates the amplification factor compared to the SAFs in this study. Previous studies [2, 20] have also highlighted this trend. Except for the very thin sediment site, NGNH20, the SAFs at the other two thick sediment sites have high amplification factors over a wide-frequency band, whereas 1DA has large amplifications only at certain frequencies. Therefore, when considering the EGM amplification in seismic design, it is necessary to use a method capable of evaluating the actual amplification factors, such as spectral inversion, rather than 1DA.

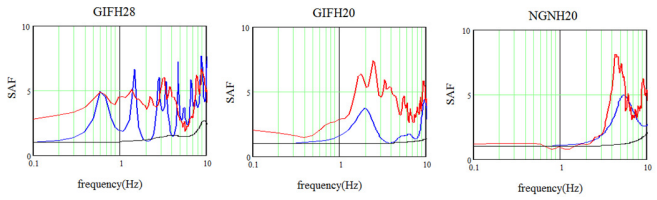

Fig. 16. SAF and 1DA.

IV. CONCLUSION

In this study, the source characteristic, path characteristic, and SAF were separated from observation records using the spectral inversion approach by utilizing the seismic records of four strong-motion observation sites in central Japan. The variation in path characteristics and SAF were quantified. The conclusions of this study are:

- SAF and path characteristic can be separated by spectral inversion by imposing a single constraint condition, namely, SAF at a hard rock site. However, the variation cannot be evaluated for the constraint condition. Therefore, the variations obtained for each characteristic contain the variation in the constraint conditions. In this study, the SD of the constraint condition was evaluated using the variation in the spectral ratio of seismograms at the ground surface to those in the borehole. The obtained SD of the constraint condition was 0.048.
- The SDs of the *SR* of two hard rock sites' records were evaluated. The variation in path characteristic was evaluated by assuming that path characteristic and SAF follow independent normal distributions. The SD of the path characteristic was estimated to be 0.121. Finally, the variation in the SAF was evaluated. The SD of the SAF was independent of the average SAF and ranged from 0.10 to 0.15 in the frequency band of 2Hz or lower. In the high-frequency band, the SD of SAF was approximately 0.30 at GIFH28 and NGNH20 and approximately 0.10 at GIFH20. The SD in the high-frequency region varies significantly from point to point. This difference in SD is due to the difference in the uniformity of the shallow subsurface around the site.
- The 1DA underestimates the SAF even when the ground structure down to the seismic bedrock is considered. At thick sediment sites, large SAF is observed in a wide-frequency band, and the envelope of the SAF is completely different from that of the 1DA. Therefore, precise evaluation of the SAF is critical for rational seismic design.

ACKNOWLEDGMENT

Strong-motion records and ground data were provided by the National Research Institute for Earth Science and Disaster Resilience. Data-sorting was aided by Yusuke Yamane. Yasuhiro Fukushima helped us evaluate the hypocentral distances.

REFERENCES

[1] N. A. Abrahamson, "State Of The Practice Of Seismic Hazard Evaluation," presented at the ISRM International Symposium, Nov. 2000, Art. no. ISRM-IS-2000-014.

[2] T. Nagao and Y. Fukushima, "Source- and Site-Specific Earthquake Ground Motions: Application of a State-of-the-Art Evaluation Method," *Engineering, Technology & Applied Science Research*, vol. 10, no. 4, pp. 5882–5888, Aug. 2020, https://doi.org/10.48084/etasr.3612.

[3] N. Morikawa *et al.*, "Strong motion uncertainty determined from observed records by dense network in Japan," *Journal of Seismology*, vol. 12, no. 4, pp. 529–546, Oct. 2008, https://doi.org/10.1007/s10950-008-9106-2.

[4] K. Kato, K. Aki, and M. Takemura, "Site amplification from coda waves: Validation and application to S-wave site response," *Bulletin of the Seismological Society of America*, vol. 85, no. 2, pp. 467–477, Apr. 1995.

[5] T. Satoh, H. Kawase, and T. Sato, "Evaluation of local site effects and their removal from borehole records observed in the Sendai region, Japan," *Bulletin of the Seismological Society of America*, vol. 85, no. 6, pp. 1770–1789, Dec. 1995.

[6] C.-H. Kuo, K.-L. Wen, C.-M. Lin, N.-C. Hsiao, and D.-Y. Chen, "Site amplifications and the effect on local magnitude determination at stations of the surface–downhole network in Taiwan," *Soil Dynamics and Earthquake Engineering*, vol. 104, pp. 106–116, Jan. 2018, https://doi.org/10.1016/j.soildyn.2017.10.003.

[7] S. S. Bora, F. Cotton, F. Scherbaum, B. Edwards, and P. Traversa, "Stochastic source, path and site attenuation parameters and associated variabilities for shallow crustal European earthquakes," *Bulletin of*

Earthquake Engineering, vol. 15, no. 11, pp. 4531–4561, Nov. 2017, https://doi.org/10.1007/s10518-017-0167-x.

[8] T. Nagao, "Seismic Amplification by Deep Subsurface and Proposal of a New Proxy," *Engineering, Technology & Applied Science Research*, vol. 10, no. 1, pp. 5157–5163, Feb. 2020, https://doi.org/10.48084/etasr. 3276.

[9] T. Nagao, "Maximum Credible Earthquake Ground Motions with Focus on Site Amplification due to Deep Subsurface," *Engineering, Technology & Applied Science Research*, vol. 11, no. 2, pp. 6873–6881, Apr. 2021, https://doi.org/10.48084/etasr.3991.

[10] Y. Fukushima and T. Nagao, "Variation of Earthquake Ground Motions with Focus on Site Amplification Factors: A Case Study," *Engineering, Technology & Applied Science Research*, vol. 9, no. 4, pp. 4355–4360, Aug. 2019, https://doi.org/10.48084/etasr.2856.

[11] T. Nagao and P. Lu, "A simplified reliability estimation method for pile-supported wharf on the residual displacement by earthquake," *Soil Dynamics and Earthquake Engineering*, vol. 129, Feb. 2020, Art. no. 105904, https://doi.org/10.1016/j.soildyn.2019.105904.

[12] D. J. Andrews, "Objective Determination of Source Parameters and Similarity of Earthquakes of Different Size," in *Earthquake Source Mechanics*, Washington DC, USA: American Geophysical Union (AGU), 1986, pp. 259–267, https://doi.org/ 10.1029/GM037p0259.

[13] T. Iwata and K. Irikura, "Source Parameters of the 1983 Japan Sea Earthquake Sequence," *Journal of Physics of the Earth*, vol. 36, no. 4, pp. 155–184, 1988, https://doi.org/10.4294/jpe1952.36.155.

[14] S. Aoi, K. Obara, S. Hori, K. Kasahara, and Y. Okada, "New strong-motion observation network : KiK-net," *Eos, Transactions, American Geophysical Union*, vol. 81, 2000.

[15] *Strong-motion seismograph networks (K-NET, KiK-net)*. https://www.kyoshin.bosai.go.jp/ (accessed Sep. 10, 2021).

[16] H. Fujiwara, S. Kawai, K. X. Hao, N. Morikawa, and H. Azuma, "J-SHIS - An integrated system for sharing information on national seismic hazard maps for Japan," in *16th World Conference on Earthquake,* Santiago Chile, Jan. 2017, Art. no. 0372.

[17] K. Aki, "Scaling law of seismic spectrum," *Journal of Geophysical Research (1896-1977)*, vol. 72, no. 4, pp. 1217–1231, 1967, https://doi.org/10.1029/JZ072i004p01217.

[18] K. Aki and P. G. Richards, *Quantitative Seismology*, 2nd ed. Mill Valley, CA, USA: University Science Books, 2009.

[19] S. Drouet, P. Triantafyllidis, A. Savvaidis, and N. Theodulidis, "Comparison of Site-Effects Estimation Methods Using the Lefkas, Greece, 2003 Earthquake Aftershocks," *Bulletin of the Seismological Society of America*, vol. 98, no. 5, pp. 2349–2363, Oct. 2008, https://doi.org/10.1785/0120080004.

[20] J. H. Steidl, A. G. Tumarkin, and R. J. Archuleta, "What is a reference site?," *Bulletin of the Seismological Society of America*, vol. 86, no. 6, pp. 1733–1748, Dec. 1996.

[21] Y. Fukushima, T. Nagao, J. Oshige, and I. Suetomi, "Ground motion evaluation for intra-plate earthquake by different site amplification factors and source models," in *7th International Conference on Earthquake Geotechnical Engineering*, Roma, Italy, Jun. 2019, pp. 2484–2492.

[22] K. Yoshimoto, H. Sato, and M. Ohtake, "Frequency-dependent attenuation of P and S waves in the Kanto area, Japan, based on the coda-normalization method," *Geophysical Journal International*, vol. 114, no. 1, pp. 165–174, Jul. 1993, https://doi.org/10.1111/j.1365-246X.1993.tb01476.x.

[23] A. Moya, J. Aguirre, and K. Irikura, "Inversion of Source Parameters and Site Effects from Strong Ground Motion Records using Genetic Algorithms," *Bulletin of the Seismological Society of America*, vol. 90, no. 4, pp. 977–992, Aug. 2000, https://doi.org/10.1785/0119990007.